UC Irvine
UC Irvine Previously Published Works

Title
The Molecular Mechanism of P2Y1 Receptor Activation.

Permalink
https://escholarship.org/uc/item/2tv8c78n

Journal
Angewandte Chemie, 55(35)

Authors
Yuan, Shuguang
Chan, H
Vogel, Horst
et al.

Publication Date
2016-08-22

DOI
10.1002/anie.201605147

Copyright Information
This work is made available under the terms of a Creative Commons Attribution-NonCommercial-NoDerivatives License, available at https://creativecommons.org/licenses/by-nc-nd/4.0/

Peer reviewed

eScholarship.org Powered by the California Digital Library
University of California

Membrane Proteins

International Edition: DOI: 10.1002/anie.201605147
German Edition: DOI: 10.1002/ange.201605147

The Molecular Mechanism of $P2Y_1$ Receptor Activation

Shuguang Yuan, H. C. Stephen Chan, Horst Vogel, Slawomir Filipek, Raymond C. Stevens,* and Krzysztof Palczewski**

Abstract: *Human purinergic G protein-coupled receptor $P2Y_1$ ($P2Y_1R$) is activated by adenosine 5′-diphosphate (ADP) to induce platelet activation and thereby serves as an important antithrombotic drug target. Crystal structures of $P2Y_1R$ revealed that one ligand (MRS2500) binds to the extracellular vestibule of this GPCR, whereas another (BPTU) occupies the surface between transmembrane (TM) helices TM2 and TM3. We introduced a total of 20 μs all-atom long-timescale molecular dynamic (MD) simulations to inquire why two molecules in completely different locations both serve as antagonists while ADP activates the receptor. Our results indicate that BPTU acts as an antagonist by stabilizing extracellular helix bundles leading to an increase of the lipid order, whereas MRS2500 blocks signaling by occupying the ligand binding site. Both antagonists stabilize an ionic lock within the receptor. However, binding of ADP breaks this ionic lock, forming a continuous water channel that leads to $P2Y_1R$ activation.*

G-protein-coupled receptors (GPCRs) participate in a wide spectrum of physiological functions by transmitting signals from an extracellular binding site to the cytoplasm. Thus, GPCRs are among the most important targets for modern therapeutics, constituting at least one third of all marketable drugs.[1] While there is considerable interest in understanding how drugs that bind to different regions of the same GPCR can produce identical responses, the molecular basis of this phenomenon remains obscure. Herein, we used $P2Y_1R$, a family A GPCR, to investigate this question. Human purinergic GPCRs are divided into two subfamilies, $P2Y_1R$-like receptors coupled to G_q proteins, and $P2Y_{12}R$-like receptors coupled to G_i proteins.[2] Both are activated by ADP to trigger glutamate release, which plays a crucial role in thrombus formation.[2] Moreover, blockade of either receptor significantly decreases ADP-induced platelet aggregation. However, inhibitors of $P2Y_1Rs$ offer a safety advantage over $P2Y_{12}R$ inhibitors by reducing the liability of bleeding.[2,3]

The $P2Y_1R$ complex crystal structures show that there are two allosteric antagonists that bind at two different regions of the receptor: 1) MRS2500 (Scheme 1; Supporting Information, Figure S1), completely blocks ADP-induced platelet aggregation, effectively decreases arterial thrombosis,[4] and binds on the surface of the ECL2 loop. 2) BPTU substantially reduces platelet aggregation[5] and binds between two helix bundles.

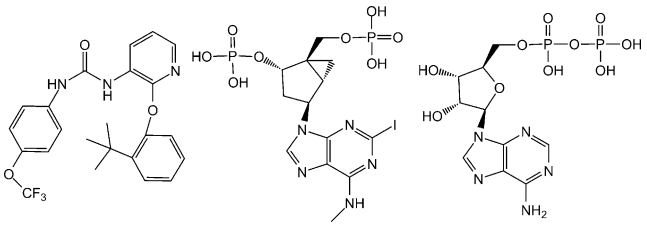

Scheme 1. Molecules used in the MD simulations.

To address structural and mechanistic questions about $P2Y_1R$, we performed a total of 20 μs atomic-level MD simulations (Table S1) on the human $P2Y_1$ receptor, starting from its crystal structures (PDB: 4XNW, 4XNV):[2] $P2Y_1R$ 1) bound to BPTU ($P2Y_1R$*-BPTU); 2) bound to MRS2500 ($P2Y_1R$-MRS2500); and 3) bound to agonist ($P2Y_1R$-ADP, $P2Y_1R$*-ADP; Figure 1). From these simulations, we con-

[*] Dr. S. Yuan, Prof. H. Vogel
Laboratory of Physical Chemistry of Polymers and Membranes
Ecole Polytechnique Fédérale de Lausanne (EPFL)
Lausanne (Switzerland)
E-mail: shuguang.yuan@gmail.com
Dr. H. C. S. Chan
Faculty of Life Sciences, University of Bradford
Bradford (UK)
Prof. S. Filipek
Laboratory of Biomodeling
Faculty of Chemistry & Biological and Chemical Research Centre
University of Warsaw
Warsaw (Poland)
Prof. R. C. Stevens
iHuman Institute
Shanghai Technical University, China and
Departments of Biological Sciences and Chemistry
University of Southern California (USA)
E-mail: stevens@usc.edu
Prof. K. Palczewski
Department of Pharmacology
School of Medicine, Case Western Reserve University
Cleveland (USA)
E-mail: kxp65@case.edu

Supporting information and the ORCID identification number(s) for the author(s) of this article can be found under http://dx.doi.org/10.1002/anie.201605147.

© 2016 The Authors. Published by Wiley-VCH Verlag GmbH & Co. KGaA. This is an open access article under the terms of the Creative Commons Attribution Non-Commercial NoDerivs License, which permits use and distribution in any medium, provided the original work is properly cited, the use is non-commercial, and no modifications or adaptations are made.

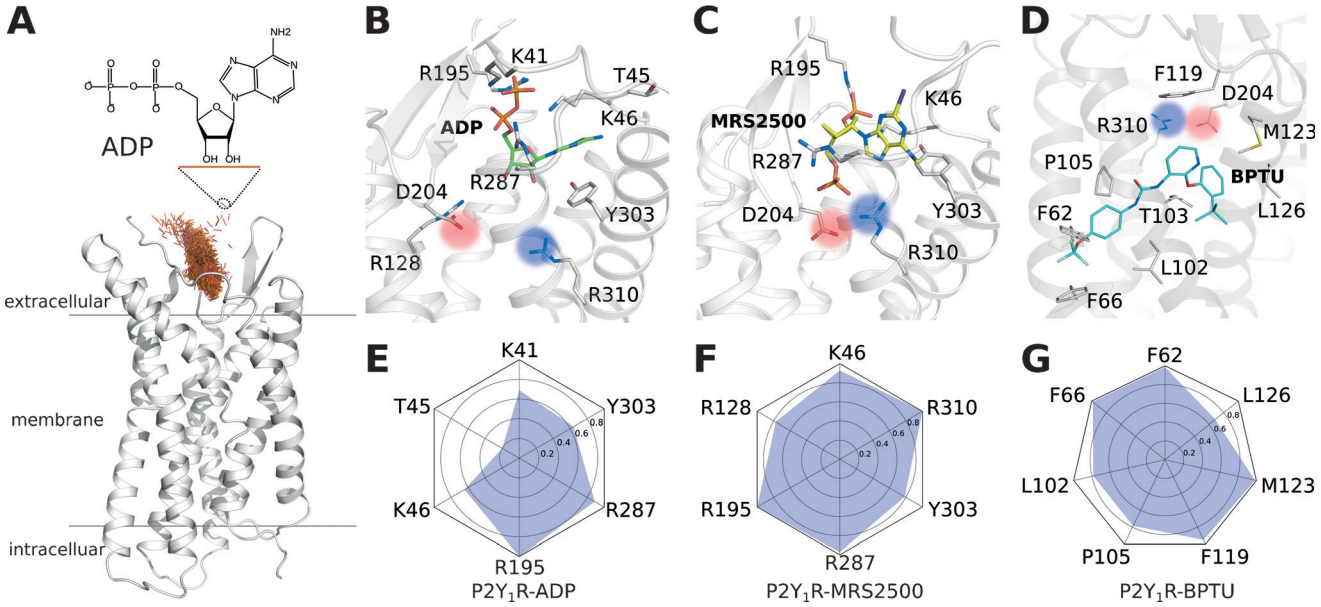

Figure 1. The ligand binding modes of $P2Y_1R$ at the end of MD simulations. A) The entrance pathway of ADP into the receptor represented as superposition of the mass centers of ADP over a time period of 0.2 μs (brown points). B) ADP binding mode. C) MRS2500 binding mode. D) BPTU binding mode. E–G) Interaction fingerprint of $P2Y_1R$ with bound ADP (E), MRS2500 (F), and BPTU (G).

clude that the two different allosteric antagonists exert their effects by either stabilizing part of the extracellular helix bundles, which lead to an increase in the lipid order (BPTU), or occupying the ligand-binding site (MRS2500). Both antagonists stabilize an ionic lock within the receptor. In contrast, the agonist molecule ADP induces breakage of the ionic lock and then formation of a continuous water channel that results in the activation of $P2Y_1R$.[6]

To sample the binding mode of the agonist molecule, we placed an ADP at the $P2Y_1R$ extracellular vestibule entrance, approximately 15 Å from the orthosteric site. Then we performed 6×2 μs all-atom long-timescale MD simulations for this system (Figure 1 A,B,E). The final poses of the ligands converged well in each simulation (Figure S2). The aromatic purine ring of ADP engaged in π-π stacking with $Y303^{7.32}$, whereas its ribose sugar ring formed an H-bond network with $Y303^{7.32}$ through the bulk water molecules. Strong interactions occurred between the negatively charged pyrophosphate and several positively charged residues, including $K41^{1.41}$, $K46^{1.46}$, $R195^{ECL2}$, and $R287^{6.38}$. This observed binding mode is consistent with extensive mutagenesis data indicating that mutations of these residues decrease the binding affinity of ADP.[2,7] We then executed 2×2 μs simulations for two additional antagonist-bound systems, namely $P2Y_1R$-MRS2500 and $P2Y_1R$*-BPTU. In antagonist-bound $P2Y_1R$-MRS2500 (Figure 1 C,F), the MRS2500 ligand located in a space similar to that of $P2Y_1R$-ADP. The substituted purine ring of MRS2500 engaged in σ-π stacking with $Y303^{7.32}$. Additionally, the 3′-phosphate formed an ionic lock with $K46^{1.46}$ and $R195^{ECL2}$, whereas the 5′-phosphate formed an ionic lock with $R287^{6.38}$ and $R310^{7.39}$. In the other antagonist-bound system, $P2Y_1R$*-BPTU (Figure 1 D,G), the ligand was located at the transmembrane (TM) helix surface far away from the classic ADP-ligand-binding site. The antagonist molecule BPTU was mainly stabilized by hydrophobic interactions with several residues, including $F62^{1.43}$, $F66^{1.47}$, $L102^{2.55}$, $P105^{2.58}$, $F119^{ECL1}$, $M123^{3.24}$, and $L126^{3.27}$. Previously, mutagenesis studies of these helix bundles revealed a reduced $P2Y_1R$-binding affinity for both antagonist ligands.[2,8]

Interestingly, we observed that an ionic lock between $D204^{ECL2}$ and $R310^{7.39}$ in agonist-bound $P2Y_1R$, was broken during the MD simulations (Figure 1 B and Figure S3 B,D). Both residues were confirmed by mutagenesis studies[5–7] as playing essential roles in $P2Y_1R$ activation. To validate whether this observation is a unique feature of agonist-bound $P2Y_1R$, we analyzed two antagonist-bound systems, namely $P2Y_1R$-MRS2500 and $P2Y_1R$*-BPTU (Figure S3 A,C). We found that this ionic lock was stabilized throughout the entire MD simulation in both $P2Y_1R$-MRS2500 and $P2Y_1R$*-BPTU, implying that the ionic lock is crucial for $P2Y_1R$ activation.

We noted that the size of the binding pocket in the agonist-bound system differed from those in the antagonist-bound states. To investigate the consequences of ligand binding, we extracted frames of the final 0.5 μs from each simulated system and analyzed its solvent accessible surface area (SASA; Figure 2). We found that the binding pocket of agonist-bound systems (Figure 2 B,D) were distinctly larger than those of the antagonist-bound states (Figure 2 A,C). Specifically, the SASA in $P2Y_1R$*-BPTU was about 3300 $Å^2$, slightly smaller than that of $P2Y_1R$-MRS2500 with a value of 3500 $Å^2$ (Figure 2 E). However, when $P2Y_1R$ bound the agonist molecule ADP, the SASA increased to 4050 and 3800 $Å^2$ in agonist-bound $P2Y_1R$*-ADP and $P2Y_1R$-ADP respectively, owing to the broken $D204^{ECL2}$-$R310^{7.39}$ ionic lock.

Because the antagonist molecule BPTU is exposed to the lipid environment between TM2 and TM3, we investigated

 © 2016 The Authors. Published by Wiley-VCH Verlag GmbH & Co. KGaA, Weinheim

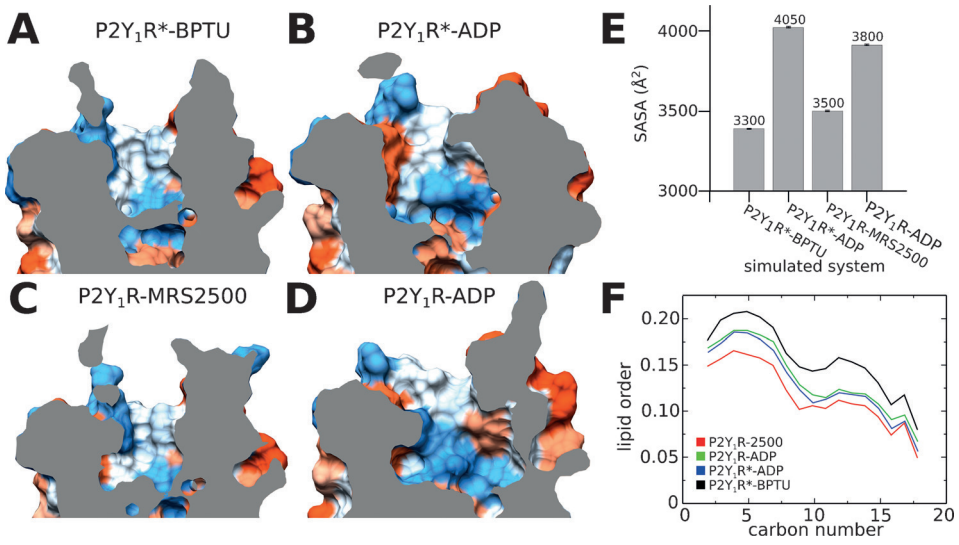

Figure 2. Solvent-accessible surface area (SASA) and lipid order of $P2Y_1R$ at the end of MD simulations. The binding pocket of $P2Y_1R$*-BPTU (A), $P2Y_1R$*-ADP (B), $P2Y_1R$-MRS2500 (C), and $P2Y_1R$-ADP (D). E) SASA values of $P2Y_1R$ calculated from the final 0.5 μs MD simulations. F) Lipid order parameters averaged over the final 0.5 μs MD simulations.

whether the binding of ligands affects the lipid order (Figure 2F). Interestingly, the lipid order was as low as 0.15 when the antagonist MRS2500 bound to the classic extracellular vestibule of $P2Y_1R$. However, when the antagonist BPTU bound to the lipid vicinity around the TM2-TM3 bundles, the lipid order increased to 0.20. Moreover, in the two agonist-bound systems $P2Y_1R$*-ADP and $P2Y_1R$-ADP, the lipid orders were identical, with a value of about 0.15. In addition, we found that the b-factor in the extracellular region of $P2Y_1R$*-BPTU was noticeably smaller than in both MRS2500- and ADP-bound $P2Y_1R$, which correlates with our lipid order observations (Figure S4). From these combined findings, we reached the following conclusions: When the allosteric antagonist BPTU attaches to the helix bundles, it stabilizes the receptor, which leads to the increased lipid order. In contrast, when MRS2500 binds to the classic extracellular vestibule, the lipid order remains relatively low and the antagonist executes its function by occupying the binding pocket. Finally, when the ADP agonist binds to the receptor, the lipid order becomes altered owing to TM movements after activation.

Water molecules have been shown to play important roles during the GPCR activation process.[6f,9] In this work, we also observed distinct water channels inside the receptor (Figure S5). In antagonist-bound $P2Y_1R$*-BPTU (Figure S5A,E), the extracellular ligand-binding pocket was filled with water molecules. However, in the intracellular zone next to the highly conserved $Y324^{7.53}$, a hydrophobic layer with a thickness of 8 Å was observed. About 12 water molecules were found within 5 Å of $Y324^{7.53}$ in $P2Y_1R$*-BPTU. In contrast, when the agonist ADP bound to the same structure ($P2Y_1R$*-ADP), it induced a continuous water channel in this region (Figure S5B,F) and the number of water molecules increased to 24 in the corresponding space. In antagonist-bound $P2Y_1R$-MRS2500, the number of water molecules stabilized at about 12 and a hydrophobic layer around 10 Å was observed. However, in the corresponding agonist system $P2Y_1R$-ADP, the number of water molecules increased to 21 and a continuous water channel also formed at the end of the MD simulations.

Furthermore, we noted that a highly conserved Tyr residue, $Y324^{7.53}$ at the NPxxY motif, underwent a conformational switch in agonist-bound $P2Y_1R$ (Figure S6). This occurred at 0.8–1.2 μs MD time scale. However, in both bound antagonists $P2Y_1R$*-BPTU and $P2Y_1R$-MRS2500, the conformation of $Y324^{7.53}$ did not change during the entire simulations. These results agree with previous findings[9] showing that $Y324^{7.53}$ plays a role as a switch, forming a continuous water channel during GPCR activation.

We also noted that the b-factor of intracellular helix bundles (Figure S4B,D) of agonist-bound systems was much higher than that of antagonist-bound systems (Figure S4A,C), implying that the intracellular helices undergo considerable movement in the activated state. In agonist-bound $P2Y_1R$, we found that several trans-membrane helixes underwent striking shifts including: TM3, ≈2 Å; TM5, ≈4 Å; TM6, ≈7 Å; and TM7 ≈5 Å (Figure 3). Because TM3, TM6, and TM7 directly contact the G_α protein and exert an essential role in

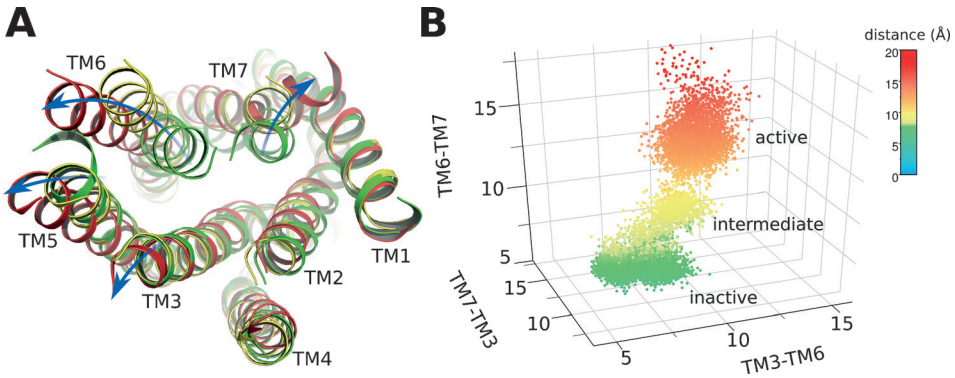

Figure 3. Helix movements of agonist-bound $P2Y_1R$. A) Helix positions of inactive (green), intermediate (yellow), and activated (red) $P2Y_1R$. B) Distances between transmembrane helix TM3, TM6, and TM7 in inactive (green), intermediate (yellow), and activated (red) receptor.

 © 2016 The Authors. Published by Wiley-VCH Verlag GmbH & Co. KGaA, Weinheim

GPCR activation,[10] we plotted the distances between different pairs of helices (Figure 3B). This strategy identified three distinct states of $P2Y_1R$ activation: the inactive, the intermediate, and the active states (Figure 3B). In the inactive state, the average distances between each TM region were low: d(TM3-TM6), 7 Å; d(TM6-TM7), 5 Å; and d(TM7-TM3), 12 Å. In the intermediate state, the average distances between each TM region increased slightly: d(TM3-TM6), 10 Å; d(TM6-TM7), 8 Å; and d(TM7-TM3), 14 Å. However, in the active state, the average distances between each TM region increased: d(TM3-TM6), 14 Å; d(TM6-TM7), 14 Å; and d(TM7-TM3), 16 Å.

Interestingly, the helix movements led to obvious changes in the residue interaction network (Figure S7). Analyses of the interactions between residue side chains revealed that in both antagonist-bound complexes $P2Y_1R$*-BPTU and $P2Y_1R$-MRS2500, most of the residues inside the receptor were in contact with multiple neighbors (Figure S7A,C). In contrast, in the agonist-bound complexes $P2Y_1R$-ADP and $P2Y_1R$*-ADP, (Figure S7B,D), interactions between the side chains inside the receptor were disrupted by helix shifting (Figure 3) and the accompanying water influx (Figure S5), dispersing the side chain interactions into smaller local groups indicative of larger inner void spaces. Residues without any contacts were found preferentially on surfaces or in loops of the receptor.

To aid in further interpretation and quantification of state-specific couplings, we constructed correlation networks in which each node represents a cluster of protein residues, and each connecting edge is weighted by the correlation value between the two clusters (Figure 4). This approach has been used successfully to unravel allosteric couplings in a range of systems.[11] In both antagonist-bound $P2Y_1Rs$ (Figure 4A,C), there were more nodes than in the agonist-bound systems: 13 nodes were found in $P2Y_1R$*-BPTU, and the same number in $P2Y_1R$-MRS2500.

However, in both agonist systems $P2Y_1R$*-ADP and $P2Y_1R$-ADP, only 8 nodes were observed. Moreover, there were fewer large nodes in antagonist systems than in agonist systems because several smaller nodes had merged after agonist binding. Specifically, the separate nodes in intracellular TM6-TM7 were grouped into a single node in the agonist-bound systems. Similar phenomena also occurred at both the extracellular section of TM6-TM7 and the intracellular section of TM2-TM4. These observations are consistent with the MD simulation results showing that intracellular TM6 and TM7 undergo the same collective motions.

In summary, on the basis of a total of 20 μs all-atom long-timescale MD simulations (Figure 5), we found that both antagonist molecules can stabilize an ionic lock between $K46^{1.46}$ and $R195^{ECL2}$ inside the receptor via different mechanisms: BPTU acts as an antagonist by stabilizing the extracellular helix bundles to increase the lipid order, whereas MRS2500 blocks signaling by occupying the ligand-binding site. The SASA of both antagonist-bound systems were smaller than the comparable agonist-bound systems. When the ADP agonist bound to the $P2Y_1R$, it induced breakage of the ionic lock and increased the SASA, inducing a bulk water influx into the binding pocket. Consequently, the rotamer of highly conserved $Y324^{7.53}$ underwent a molecular switch and a continuous water channel formed inside the receptor. Finally, TM3, TM6, and TM7 shifts in the cytoplasmic region

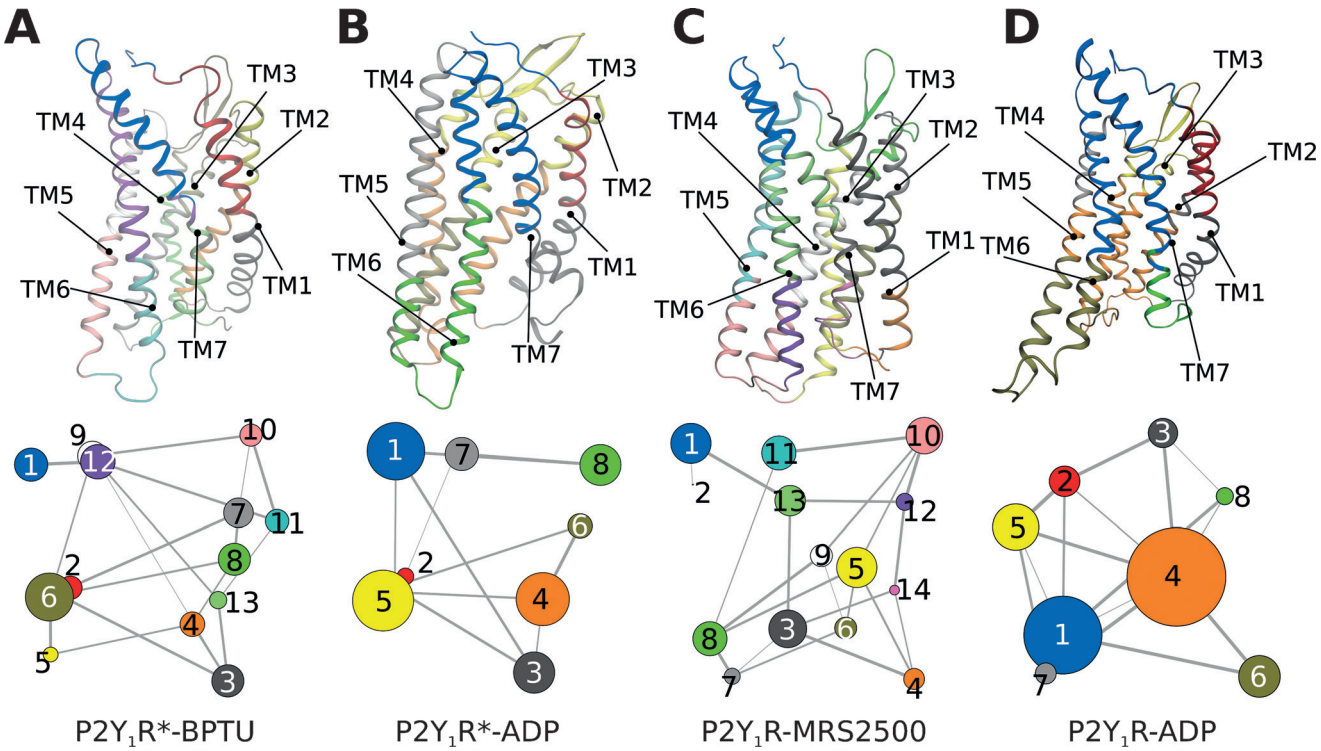

Figure 4. Simultaneous view of the community residue interaction network and 3D structures of A) $P2Y_1R$*-BPTU, B) $P2Y_1R$*-ADP, C) $P2Y_1R$-MRS2500, and D) $P2Y_1R$-ADP.

 © 2016 The Authors. Published by Wiley-VCH Verlag GmbH & Co. KGaA, Weinheim

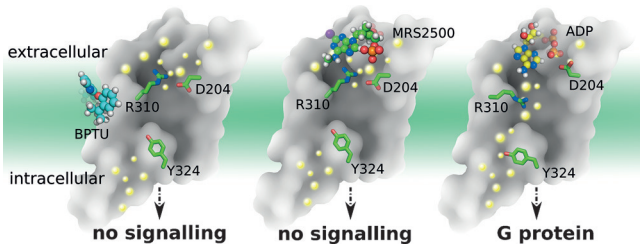

Figure 5. Molecular mechanism of action inferred from the $P2Y_1R$ structure. The big dots represent water molecules close to the front on the Figure, whereas the smaller dots indicate water molecules further away. Left panel: Antagonist molecule BPTU binds to $P2Y_1R$ and stabilizes the ionic lock between $K46^{1.46}$ and $R195^{ECL2}$ inducing a decrease in the lipid order. No continuous internal water channel is formed. Middle panel: Antagonist molecule MRS2500 binds to $P2Y_1R$ and stabilizes the ionic lock between $K46^{1.46}$ and $R195^{ECL2}$. No continuous internal water channel is formed. Right panel: Agonist molecule ADP binds to $P2Y_1R$ and disrupts the ionic lock between $K46^{1.46}$ and $R195^{ECL2}$. $Y324^{7.53}$ undergoes a molecular switch that results in the formation of a continuous water channel inside the receptor.

created a large void for G protein binding with subsequent activation of the receptor. These findings provide new insights into the molecular changes and actions of GPCR allosteric ligands. Such insights are applicable to innovative drug discovery.

Experimental Section

MD simulations. All membrane systems were built with the membrane building tool in Schrodinger Maestro[12] software with each receptor structure pre-aligned in the OPM (Orientations of Proteins in Membranes) database.[13] Pre-equilibrated 128 POPC lipids coupled with 9,800 TIP3P water molecules in a periodic box of 70 Å × 70 Å × 96 Å were used to build the protein/membrane system. Proteins, lipids, water molecules and ions were modelled with the CHARMM36 force field[14] parameter set, and the ligands were modelled with the CHARMM CGenFF small molecule force field.[15] All of the ligands were submitted to the GAUSSIAN 09 program[16] for structure optimization at the B3LYP/6-31G* level prior to force field parameter generation. All of the bond lengths to hydrogen atoms in each protein/membrane system were constrained with M-SHAKE.[17] Van der Waals and short-range electrostatic interactions were cut off at 10 Å. Results obtained from the MD simulations were analyzed in Gromacs[18] and VMD.[19]

Acknowledgements

We thank the Interdisciplinary Centre for Mathematical and Computational Modelling in Warsaw (grant G07-13), providing the major computing part of this project (grant BIO120006P). Part of the work was performed at the Pittsburgh Supercomputing Center in the USA for use of the Anton supercomputer system (NIH grant R01GM116961). S.F. received funding from the National Center of Science, Poland, grant no. 2013/08/M/ST6/00788. Research in H.V.'s group was supported by the European Community (project SynSignal, grant no. FP7-KBBE-2013-613879), and internal funds of the EPFL. K.P. was supported by the Arnold and Mabel Beckman Foundation. H.V. and S.F. participate in the European COST Action CM1207 (GLISTEN). We also thank the Canadian Institute for Advanced Research (CIFAR). K.P. is the John H. Hord Professor of Pharmacology.

Keywords: activation mechanism · allosteric ligand · GPCR · molecular switches · $P2Y_1R$

How to cite: *Angew. Chem. Int. Ed.* **2016**, *55*, 10331–10335
Angew. Chem. **2016**, *128*, 10487–10491

[1] a) D. Wootten, et al., *Nat. Rev. Drug Discovery* **2013**, *12*, 630; b) J. Li, et al., *J. Am. Chem. Soc.* **2013**, *135*, 8749; c) A. S. Rose, et al., *PLoS One* **2015**, *10*, e0143399.
[2] D. Zhang, et al., *Nature* **2015**, *520*, 317.
[3] C. Gachet, *Thromb. Haemostasis* **2008**, *99*, 466.
[4] B. Hechler, et al., *J. Pharmacol. Exp. Ther.* **2006**, *316*, 556.
[5] H. Chao, et al., *J. Med. Chem.* **2013**, *56*, 1704.
[6] a) S. K. Lakkaraju, et al., *J. Comput. Chem.* **2016**, *37*, 416; b) M. Schneider, et al., *FEBS Lett.* **2011**, *585*, 3587; c) A. S. Rose, et al., *J. Am. Chem. Soc.* **2014**, *136*, 11244; d) R. Nygaard, et al., *Cell* **2013**, *152*, 532; e) S. Yuan, et al., *Angew. Chem. Int. Ed.* **2015**, *54*, 556; *Angew. Chem.* **2015**, *127*, 566; f) S. Yuan, et al., *Nat. Commun.* **2014**, *5*, 4733.
[7] S. Moro, et al., *Biochemistry* **1999**, *38*, 3498.
[8] a) D. Guo, et al., *Drug Dev. Res.* **2002**, *57*, 173; b) S. Moro, et al., *J. Med. Chem.* **1998**, *41*, 1456.
[9] a) S. Yuan, et al., *Angew. Chem. Int. Ed.* **2015**, *54*, 7560; *Angew. Chem.* **2015**, *127*, 7670; b) S. Yuan, et al., *Angew. Chem. Int. Ed.* **2013**, *52*, 10112; *Angew. Chem.* **2013**, *125*, 10299; c) W. Liu, et al., *Science* **2012**, *337*, 232; d) T. E. Angel, et al., *Proc. Natl. Acad. Sci. USA* **2009**, *106*, 14367; e) F. Garczarek, K. Gerwert, *Nature* **2006**, *439*, 109; f) S. Yuan, et al., *Angew. Chem. Int. Ed.* **2016**, *55*, 8661; *Angew. Chem.* **2016**, *128*, 8803.
[10] a) B. Trzaskowski, et al., *Curr. Med. Chem.* **2012**, *19*, 1090; b) T. Flock, et al., *Nature* **2015**, *524*, 173.
[11] a) Y. Karami, et al., *BMC Bioinf.* **2016**, *17*, 13; b) L. Skjaerven, et al., *BMC Bioinf.* **2014**, *15*, 399; c) S. Yuan, et al., *Structure* **2016**, *24*, 816.
[12] Schrödinger, Schrödinger, LLC, **2015**.
[13] M. A. Lomize, et al., *Bioinformatics* **2006**, *22*, 623.
[14] J. B. Klauda, et al., *J. Phys. Chem. B* **2010**, *114*, 7830.
[15] K. Vanommeslaeghe, et al., *J. Chem. Inf. Model.* **2012**, *52*, 3155.
[16] M. J. Frisch, et al., Gaussian, Inc., Wallingford, CT, USA, **2009**.
[17] R. Schmauder, et al., *ChemBioChem* **2011**, *12*, 2431.
[18] S. Pronk, et al., *Bioinformatics* **2013**, *29*, 845.
[19] W. Humphrey, et al., *J. Mol. Graphics Modell.* **1996**, *14*, 33.

Received: May 26, 2016
Revised: June 27, 2016
Published online: July 27, 2016

 © 2016 The Authors. Published by Wiley-VCH Verlag GmbH & Co. KGaA, Weinheim